A NATURAL NEIGHBOR BASED MOVING LEAST SQUARES APPROACH WITH INTERPOLATING WEIGHTING FUNCTION

T. Most, C. Bucher and M. Macke

Institute of Structural Mechanics
Bauhaus-University Weimar, Germany
E-mails:thomas.most@uni-weimar.de
christian.bucher@uni-weimar.de
michael.macke@uni-weimar.de

Keywords: Meshless method, Moving Least Squares, Element-free Galerkin, Interpolation condition, Adapted influence domains, Natural neighbor nodes

Abstract. *In this paper two enhancements of the classical Moving Least Squares approach will be presented. The first one is an interpolating weighting function, which leads to MLS shape functions fulfilling the interpolation condition exactly. This enables a direct application of essential boundary conditions without additional numerical effort. In contrast to existing approaches using singular weighting functions, this new weighting type leads to regular values of the weights and coefficients matrices in the whole domain even at the support points.*

The second approach is the adaptation of the nodal influence domains according to the nodal configuration. For this purpose the influence radius is interpolated depending on the direction from the distances to the natural neighbor nodes. This leads to a more uniform and reduced number of influencing nodes for systems with grading node density than with the classical circular influence domains. Furthermore the numerical effort of the analysis will be reduced significantly.

1   INTRODUCTION

The Element-free Galerkin Method [1] has become a very popular tool for the simulation of mechanical problems with moving boundaries. The internally applied Moving Least Squares approximation [2] uses in general Gaussian or cubic weighting functions and has compact support. Due to the approximative character of this method the obtained shape functions do not fulfill the interpolation condition, which causes additional numerical effort for the imposition of the essential boundary conditions. The application of a singular weighting function, which leads to singular coefficient matrices at the nodes, can solve this problem, but requires a very careful placement of the integration points. In [3] and [4] special procedures for the handling of such singular matrices were proposed, which require additional numerical effort. In this paper a non-singular weighting function is presented, which leads to an exact fulfillment of the interpolation condition. This weighting function leads to regular values of the weights and the coefficient matrices in the whole interpolation domain even at the nodes. Furthermore this function gives much more stable results for varying size of the influence radius and for strongly distorted nodal arrangements than classical weighting function types.

Finally a new concept will be presented, which enables an efficient analysis of systems with strongly varying node density. In this concept the nodal influence domains are adapted depending on the nodal configuration by interpolating the influence radius for each direction from the distances to the natural neighbor nodes. This approach requires a Voronoi diagram of the domain, which is available in this study since Delaunay triangles are used as integration background cells. In the numerical examples it will be shown, that this enhanced method leads to similar results as the classical approach, but will reduce the numerical effort significantly.

2   MOVING LEAST SQUARES APPROACH (MLS)

An arbitrary function u is interpolated at a point $\mathbf{x}$ by a polynomial as

$$u^h(\mathbf{x}) = \begin{bmatrix} 1 & x & y & x^2 & xy & y^2 & ... \end{bmatrix} \begin{bmatrix} a_1 \\ \vdots \\ a_n \end{bmatrix} = \mathbf{p}^T(\mathbf{x})\mathbf{a} \qquad (1)$$

where $\mathbf{p}(\mathbf{x})$ is the base vector and $\mathbf{a}$ contains the coefficients of the polynomial. These coefficients are constant in the interpolation domain and can be determined directly if the number of supporting points m used for the interpolation is equivalent to the number of coefficients n. This principle is applied for example in the Finite Element Method, where an element-wise interpolation is realized. There the coefficients are simply given as

$$\mathbf{a} = \mathbf{P}^{T^{-1}}\tilde{\mathbf{u}} \qquad (2)$$

where $\tilde{\mathbf{u}}$ contains the function values at the supporting points

$$\tilde{\mathbf{u}} = \begin{bmatrix} \tilde{u}_1 & ... & \tilde{u}_m \end{bmatrix}^T \qquad (3)$$

and $\mathbf{P}$ consists of the values of the polynomial basis calculated at the supporting points

$$\mathbf{P} = \begin{bmatrix} P_1(\mathbf{x}_1) & P_1(\mathbf{x}_2) & \dots & P_1(\mathbf{x}_m) \\ P_2(\mathbf{x}_1) & P_2(\mathbf{x}_2) & \dots & P_2(\mathbf{x}_m) \\ \vdots & \vdots & \ddots & \vdots \\ P_n(\mathbf{x}_1) & P_n(\mathbf{x}_2) & \dots & P_n(\mathbf{x}_m) \end{bmatrix}. \qquad (4)$$

2

Within the "Moving Least Squares" (MLS) approximation method [2] the number of supporting points m exceeds the number of coefficients n, which leads to an overdetermined system of equations. This kind of optimization problem can be solved by using a least squares approach

$$\mathbf{P}\tilde{\mathbf{u}} = \mathbf{P}\mathbf{P}^T\mathbf{a}(\mathbf{x}) \tag{5}$$

with changing ("moving") coefficients $\mathbf{a}(\mathbf{x})$. In order to obtain a compact support and a local character of the MLS-approach a distance depending weighting function $w = w(s)$ was introduced, where s is the normalized distance between the interpolation point and the considered supporting point

$$s_i = \frac{\|\mathbf{x} - \mathbf{x}_i\|}{D} \tag{6}$$

and D is the influence radius, which is defined as a numerical parameter. All types of functions can be used as weighting function $w(s)$ which have their maximum in $s = 0$ and vanish outside of the influence domain specified by $s = 1$. The nodes whose weighting function values do not vanish at the interpolation point are the influencing nodes of the interpolation point.

Using the introduced weighting function, Eq. (5) is expanded to

$$\mathbf{B}(\mathbf{x})\tilde{\mathbf{u}} = \mathbf{A}(\mathbf{x})\mathbf{a}(\mathbf{x}), \tag{7}$$

where $\mathbf{A}(\mathbf{x})$ and $\mathbf{B}(\mathbf{x})$ are given as

$$\begin{aligned} \mathbf{A}(\mathbf{x}) &= \mathbf{P}\mathbf{W}(\mathbf{x})\mathbf{P}^T, \\ \mathbf{B}(\mathbf{x}) &= \mathbf{P}\mathbf{W}(\mathbf{x}), \end{aligned} \tag{8}$$

and the diagonal matrix $\mathbf{W}(\mathbf{x})$ can be determined as

$$\mathbf{W}(\mathbf{x}) = \begin{bmatrix} w(\mathbf{x} - \mathbf{x}_1) & 0 & \dots & 0 \\ 0 & w(\mathbf{x} - \mathbf{x}_2) & \dots & 0 \\ \vdots & \vdots & \ddots & \vdots \\ 0 & 0 & \dots & w(\mathbf{x} - \mathbf{x}_m) \end{bmatrix}. \tag{9}$$

The interpolated value of the function u at $\mathbf{x}$ can be obtained by introducing the MLS shape functions

$$u^h(\mathbf{x}) = \boldsymbol{\Phi}^{MLS}(\mathbf{x})\tilde{\mathbf{u}}, \quad \boldsymbol{\Phi}^{MLS}(\mathbf{x}) = \mathbf{p}^T(\mathbf{x})\mathbf{A}(\mathbf{x})^{-1}\mathbf{B}(\mathbf{x}). \tag{10}$$

Similar to Eq. (2) the invertibility of the matrix $\mathbf{A}(\mathbf{x})$ has to be assured, which is not automatically given if the interpolation point is in the influence domain of at least n nodes. This is fulfilled for a linear or quadratic polynomial basis in 2D if these nodes span two or three linear independent vectors, respectively, as derived in [5].

In contrast to the Finite Element Method the MLS approximation does not pass through the nodal values caused by the applied least squares approach. This implies that the interpolation condition is not fulfilled,

$$\Phi_i^{MLS}(\mathbf{x}_j) \neq \delta_{ij}. \tag{11}$$

3 WEIGHTING FUNCTIONS

A large number of different weighting functions for the Moving Least Squares approach can be found in the literature. In this section one of the most common weighting type, the Gaussian weighting function, is shortly discussed. This weighting function is of exponential type and is given e.g. in [5] as

$$
w_G(s) = \begin{cases} \dfrac{e^{-\frac{s^2}{\alpha^2}} - e^{-\frac{1}{\alpha^2}}}{1 - e^{-\frac{1}{\alpha^2}}} & s \leq 1 \\ 0 & s > 1 \end{cases}.
$$
(12)

In Fig. 1 the Gaussian weighting function is displayed for the one-dimensional case. Due to the applied least square approach explained in the previous section, the obtained nodal shape functions have a strong dependence on the size of the influence radius D. In Fig. 2 a single nodal shape function of the middle node of a regular one-dimensional set of nodes is shown for increasing D. The figure indicates that with increasing influence radius, the shape function error at each support point, caused by the approximative character of the MLS approach, increases dramatically. This problem is even more significant for irregular nodal setups. As a result the application of geometrical boundary conditions is difficult and additional numerical effort is necessary to fulfill these conditions.

Because of the presented problems using classical weighting function types, in [6] the authors presented a regularized weighting function which enables the fulfillment of the MLS interpolation condition with very high accuracy without additional numerical effort

$$
\Phi_i^{MLS}(\mathbf{x}_j) \approx \delta_{ij}.
$$
(13)

The weighting function value of a node i at an interpolation point $\mathbf{x}$ was introduced as follows

$$
w_R(s) = \frac{\tilde{w}_R(s)}{\displaystyle\sum_{j=1}^{m} \tilde{w}_R(s_j)}
$$
(14)

with

$$
\tilde{w}_R(s) = \frac{(s^\gamma + \epsilon)^{-2} - (1 + \epsilon)^{-2}}{\epsilon^{-2} - (1 + \epsilon)^{-2}}; \quad \epsilon \ll 1.
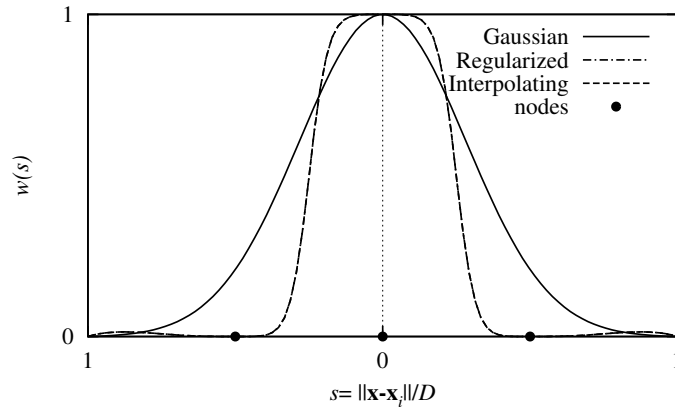$$
(15)

Figure 1: Gaussian, regularized and new interpolating weighting functions for a single node with neighbor nodes

4

Gaussian weight
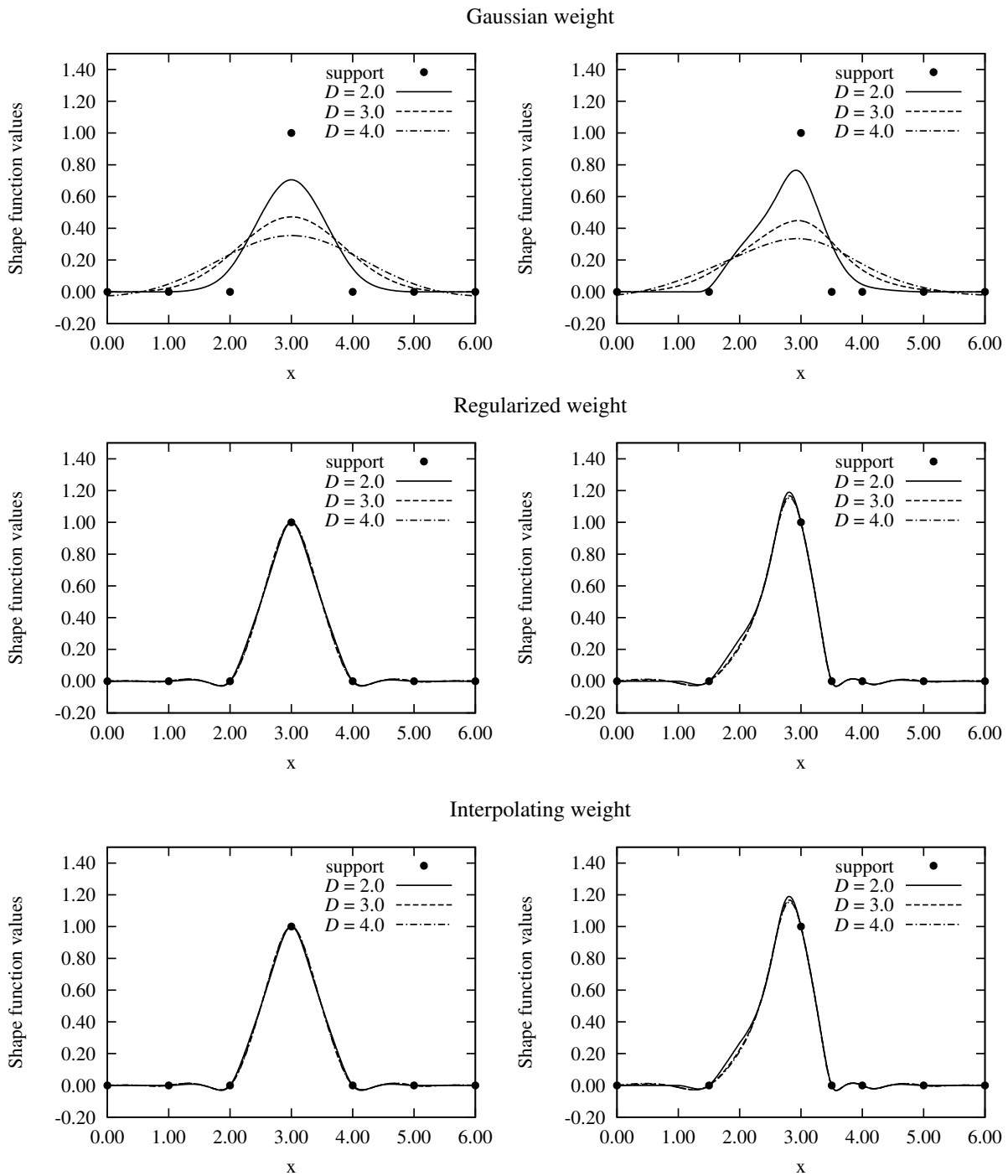

Regularized weight

Interpolating weight

Figure 2: Nodal shape function of the MLS interpolation with Gaussian, regularized and interpolating weighting function and linear polynomial basis for regular and irregular sets of nodes

5

In [6] it is recommended to choose the regularization parameter ϵ as

$$\epsilon = 10^{-5} \tag{16}$$

and the exponent in Eq. (15) is taken as $\gamma = 2$. In Fig. 1 the regularized weighting function is displayed additionally as a function of the standardized distance s and the position of the supporting points. In Fig. 2 a single nodal shape function obtained by using the regularized weighting function type is shown for different values of the influence radius D. The figure clearly points out that the interpolation condition is fulfilled with very high accuracy even for irregular sets of nodes with grading node density. In clear contrast to the shape functions obtained with the Gaussian weighting function the influence radius D influences the regularized shape function characteristics marginally if a certain value of D is reached.

In this paper the regularized weighting type is enhanced in order to obtain a true interpolation MLS approach. Based on the following formulation

$$w_I(s) = \frac{s^{-\alpha} - 1}{\displaystyle\sum_{j=1}^{m}(s_j^{-\alpha} - 1)}, \tag{17}$$

which can not be evaluated numerically at the support points, the following final weighting function is formulated

$$w_I(s) = \frac{s_i^{\alpha}(s^{-\alpha} - 1)}{s_i^{\alpha}\displaystyle\sum_{j=1}^{m}(s_j^{-\alpha} - 1)}, \tag{18}$$

where s_i denotes the distance to the closest support point. Eq. (18) can be simplified as

$$w_I(s_i) = \frac{1 - s_i^{\alpha}}{1 + s_i^{\alpha}\displaystyle\sum_{j=1,j\neq i}^{m} s_j^{-\alpha} + s_i^{\alpha}m}; \qquad w_I(s_{i\neq j}) = \frac{s_i^{\alpha}(s_j^{-\alpha} - 1)}{1 + s_i^{\alpha}\displaystyle\sum_{j=1,j\neq i}^{m} s_j^{-\alpha} + s_i^{\alpha}m}. \tag{19}$$

If no pair of support points with equal positions exists, the weighting function in Eq. (19) provides always regular numerical values even at all support points, where we obtain

$$w_I(s_i = 0) = 1; \qquad w_I(s_{i\neq j}) = 0. \tag{20}$$

In this paper the exponent is chosen as $\alpha = 4$. In Fig. 1 and Fig. 2 the shape functions using this interpolating weighting type are displayed, which show no visible deviation to the shape functions using the almost interpolating regularized weighting type. In the first example the differences in the numerical results between both weighting types are investigated.

6

4 NODAL INFLUENCE DOMAINS
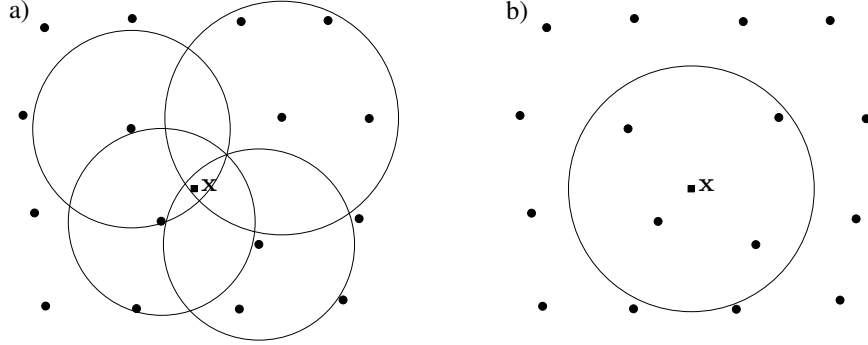
4.1 Circular influence domains

Figure 3: Neighbor search a) from the nodal positions with varying D and b) from the interpolation point with unique D
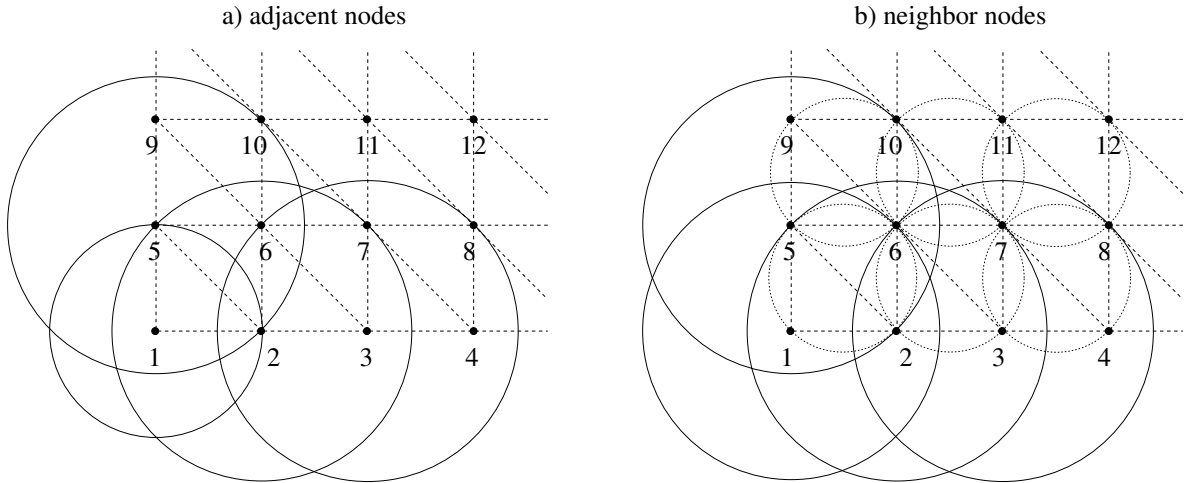

Figure 4: Influence domain with $\beta = 1.01$ using the maximum distance a) to the adjacent nodes and b) to the natural neighbor nodes

The distance depending weighting function type leads to circular and spherical influence domains in two and three dimensions, respectively. Alternatively to this type, rectangular or other shaped influence domains have been applied [7], but the distance depending type is more general and mostly realized in efficient implementations. If the influence radius D is assumed to be equal for all nodes, the influencing nodes can be determined directly from the interpolation point, which is shown in Fig. 3b. For a varying D the neighbor search has to be performed from the nodes as shown in Fig. 3a. For domains with grading node density the influence radius of each node D_I is assumed generally in that way, that a given number of the other nodes is covered by the influence domain. This may lead to some problems in the corners of a domain, which will be shown in the final numerical example. In [8] an improved concept is proposed, whereby the influence radius is chosen to be

$$D_I = \beta \cdot r_{I_{max}}, \quad \beta > 1, \tag{21}$$

7

with

$$r_{I_{max}} = \max \|\mathbf{x}_i - \mathbf{x}_I\|, \quad i \in J_I^A, \tag{22}$$

where J_I^A represents the set of adjacent nodes. The adjacent nodes are these nodes, which span a triangular integration cell with the node I. In Fig. 4a the resulting influence domains of some regular distributed nodes are shown.

In this work triangular integration cells are used similarly to [8], which are computed here using a constrained Delaunay triangulation [9]. For cases where the Delaunay triangulation is not unique, e.g. for regular nodal configurations as shown in Fig. 4, the maximum distance of the adjacent nodes is not unique as well and leads to non-uniform influence radii for uniform nodal positions. This lack is fixed in this work by taken the set of natural neighbor nodes J_I^N instead of the adjacent nodes J_I^A for the determination of the maximum distance. Neighbor nodes of I are these nodes, which share a common edge with I in the Voronoi diagram [10]. The natural neighbor nodes can be simply obtained by the determination of these Delaunay triangles, which have the node I on their circumcircle. All nodes which span these triangles are the natural neighbor nodes of I. The obtained nodal influence domains are always unique since the Voronoi diagram is unique. In Fig. 4b it is shown, that the influence domains have the same size for a regular set of nodes.

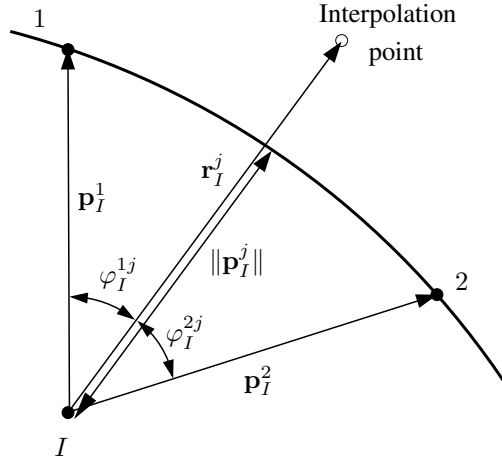## 4.2 Adapted influence domains using interpolated neighbor node distances

Figure 5: Interpolation of the nodal distances

For problems with strongly varying node density, the above explained circular influence domains may lead to a large number of influencing nodes in the part of the structure with the larger density, since the influence radius is unique in all directions. This results in a larger numerical effort for the affected integration points, since the MLS operations are more time consuming with increasing number of influencing nodes. In this paper a new concept is presented, where the influence radius of each node is formulated depending on the direction,

$$D_I \left(\frac{\mathbf{r}_I^j}{\|\mathbf{r}_I^j\|} \right) = \beta \cdot \|\mathbf{p}_I^j\|, \quad \beta > 1, \tag{23}$$

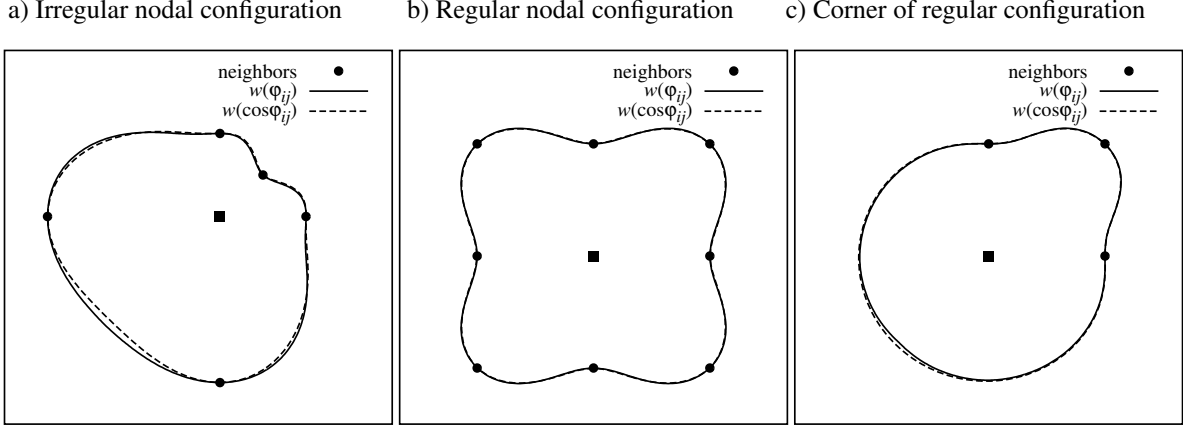a) Irregular nodal configuration   b) Regular nodal configuration   c) Corner of regular configuration

Figure 6: Adapted nodal influence domains using interpolated neighbor node distances

where $\|\mathbf{p}_I^j\|$ is the actual radius obtained by interpolating the distances of all natural neighbor nodes J_I^N to the actual node I. This is realized here by an interpolation scheme using weighted radii, which was proposed in [11] for response surface applications and is based on the Shepard interpolation [12]. By applying this approach the actual radius reads

$$\|\mathbf{p}_I^j\| = \frac{\sum_i \|\mathbf{p}_I^i\| w_I^{ij}}{\sum_i w_I^{ij}}, \quad i \in J_I^N, \tag{24}$$

where is $\|\mathbf{p}_I^i\|$ is the distance of the neighbor node i to the actual investigated node I. The weighting function values w_I^{ij} have been introduced in [11] as

$$w_I^{ij} = \left[\varphi_I^{ij} + \epsilon\right]^{-2}, \quad 0 \leq \varphi_I^{ij} \leq \pi, \tag{25}$$

where φ_I^{ij} is the enclosed angle between the vectors from the node I to the interpolation point and to the neighbor node i (Fig. 5) and ϵ is again a regularization parameter, which is taken here as $\epsilon = 10^{-5}$. In Fig. 6 the resulting influence domains are shown for irregular and regular nodal configurations. The enclosed angle φ_I^{ij} is obtained in [11] from

$$\cos\varphi_I^{ij} = \frac{\mathbf{p}_I^{iT} \mathbf{r}_I^j}{\|\mathbf{p}_I^i\| \|\mathbf{r}_I^j\|}. \tag{26}$$

In this paper a slightly modified weighting function is used

$$w_I^{ij} = \left[1 - \cos\varphi_I^{ij} + \epsilon\right]^{-1}, \tag{27}$$

which leads to similar influence domains as the function in Eq. (25), but requires less operations especially for the computation of the derivatives of the nodal shape functions. Fig. 6 shows additionally the influence domains using Eq. (27). Both formulations in Eq. (25) and Eq. (27) lead to a at least C^2 continuous function for D_I.

If the scaling factor in Eq. (23) is chosen as $\beta = 1$ the number of influencing nodes for each interpolation point is at least three, which are the three nodes spanning the Delaunay triangle containing the interpolation point, except at the nodes, where only the node itself has a nonzero shape function value. This is similar as in the Natural Neighbor Interpolation [13]. For the application in the MLS approach it is necessary to choose $\beta > 1$ in order to obtain smooth nodal shape functions.

5 NUMERICAL EXAMPLES

5.1 MLS-shape functions for regular and irregular sets of nodes

Within this example the interpolation errors are calculated for a regular and an irregular set of 5×5 nodes with a distance of $a = 0.25m$ by using the Gaussian, the regularized and the interpolating weighting functions. In Fig. 7 both investigated nodal sets are displayed.
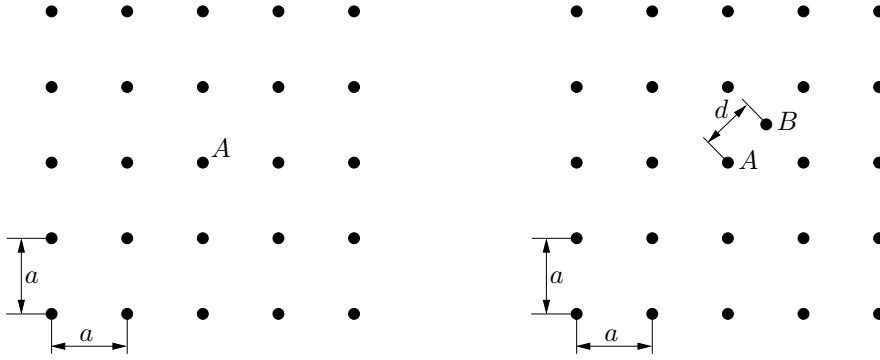
Figure 7: Investigated regular and irregular sets of nodes

First the interpolation error at the supporting points for the shape function of node A is analyzed for a varying influence radius D using the regular nodal set. The regularization term for the regularized weighting function is assumed to be $\epsilon = 10^{-5}$ and the Gaussian shape parameter is taken with $\alpha = 0.3295$. In Table 1 the obtained maximum error is given for all investigated

D	$\left|\Phi_{i,G}^{MLS}\left(\mathbf{x}_j\right) - \delta_{ij}\right|_{max}$	$\left|\Phi_{i,R}^{MLS}\left(\mathbf{x}_j\right) - \delta_{ij}\right|_{max}$	$\left|\Phi_{i,I}^{MLS}\left(\mathbf{x}_j\right) - \delta_{ij}\right|_{max}$
0.3 m	0.6 %	$4.29 \cdot 10^{-8}$ %	0
0.4 m	10.1 %	$2.48 \cdot 10^{-7}$ %	0
0.5 m	30.5 %	$7.20 \cdot 10^{-7}$ %	0
0.6 m	49.5 %	$1.65 \cdot 10^{-6}$ %	0
1.0 m	81.5 %	$1.42 \cdot 10^{-5}$ %	0

Table 1: Maximum interpolation error at the nodes as a function of the influence radius using Gaussian (G), regularized (R) and interpolating (I) weighting types

weighting types. It can be seen, that with increasing influence radius the error using the Gaussian weighting function increases but the error from the regularized type remains very small. Furthermore the interpolating weighting type leads to exact fulfillment of the interpolation condition.

The influence of the minimum nodal distance on the interpolation accuracy is investigated on the irregular set of nodes shown in Fig. 7 by decreasing the distance between node A and B. The influence radius is kept constant with $D = 0.5m$. In Table 2 the obtained interpolation errors are shown. The table clearly indicates that the interpolation error by using the regularized weighting function is very small for larger values of d_{AB}/D and increases for decreasing minimum nodal distance. The application of the interpolating weighting function leads again to an exactly fulfilled interpolation condition.

d_{AB}/D	$\left|\Phi_{i,G}^{MLS}\left(\mathbf{x}_j\right)-\delta_{ij}\right|_{max}$	$\left|\Phi_{i,R}^{MLS}\left(\mathbf{x}_j\right)-\delta_{ij}\right|_{max}$	$\left|\Phi_{i,I}^{MLS}\left(\mathbf{x}_j\right)-\delta_{ij}\right|_{max}$
0.4	36.8 %	$9.61\cdot10^{-7}$ %	0
0.2	47.7 %	$2.57\cdot10^{-6}$ %	0
0.1	55.2 %	$1.02\cdot10^{-5}$ %	0
0.01	59.0 %	$1.05\cdot10^{-3}$ %	0
0.001	59.0 %	$1.05\cdot10^{-1}$ %	0

Table 2: Maximum numerical error as a function of the minimum nodal distance

5.2 Patch test with irregular nodal distribution

The representation of a linear displacement field depending on the integration density is analyzed in this example. For this investigation a system according to [14] is chosen, which is shown with load and boundary conditions in Fig. 8. The thickness of the panel is taken as $d = 1m$ and the material properties are assumed to be $E = 10^5 N/m^2$ for the Young's modulus and $\nu = 0.2$ for the Poisson's ratio. The application of the boundary tractions on the left side is
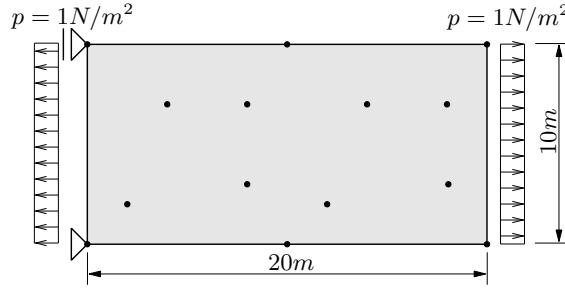

Figure 8: Patch test system with loading and boundary conditions

necessary due to the only point-wise fulfillment of the essential boundary conditions.

In Fig. 9 the obtained maximum displacement error at the nodes is shown depending on the number of equally weighted integration points per triangular background cell. The calculations are carried out with a linear basis and by choosing $D = 15m$. The figure clearly indicates,
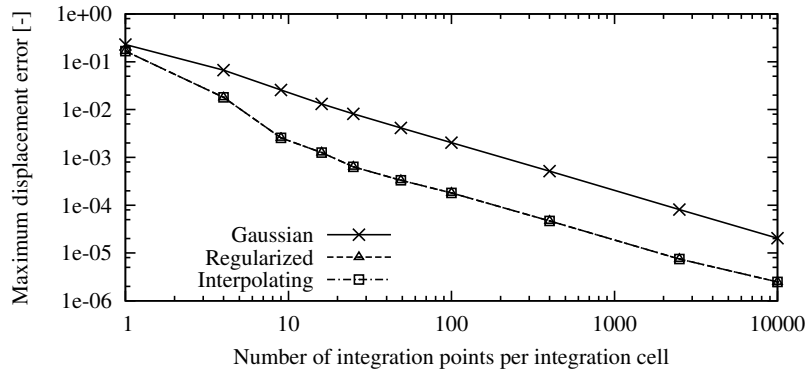

Figure 9: Maximum nodal displacement error for the patch test depending on the number of integration points

that the integration error decreases with increasing integration order for all three weighting types. The results using the regularized and the interpolating weighting function show no visible difference.
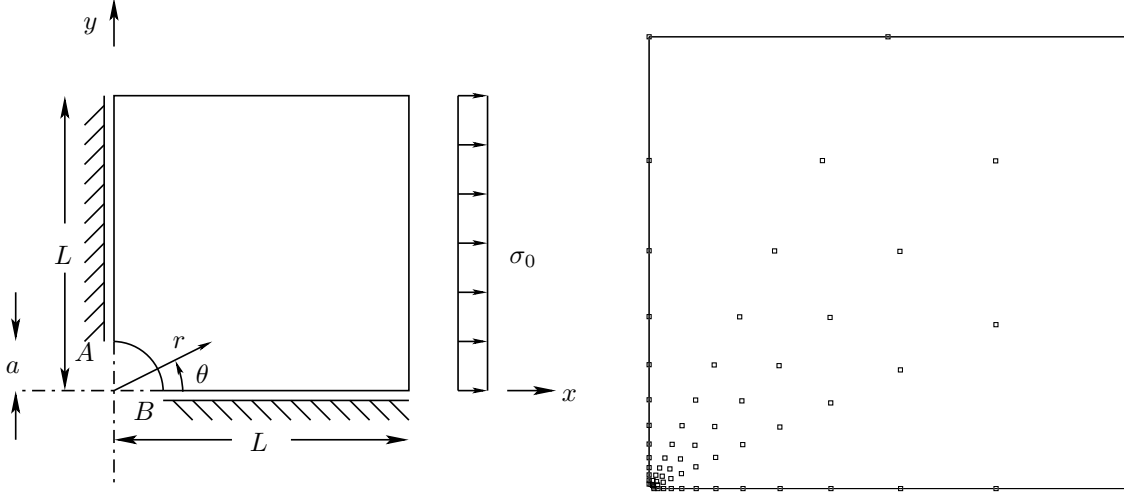
11

5.3 Infinite plate with a hole

Figure 10: Infinite plate with a hole and investigated meshless discretization with 65 nodes

In this example an infinite plate with a hole is investigated under tension loading. The benchmark example was proposed by [15]. It has been chosen here to investigate the differences between the presented nodal influence domains. In Fig. 10 the system with loading and boundary conditions is shown. Due to the symmetry of the plate, in the numerical analysis only one quarter is discretized. In order to approximate an infinite plate the ratio between the hole radius a and the half plate length L is taken very small as $a/L = 0.01$. The analytical displacement solution is given in [15] as

$$
\begin{aligned}
u_x(r,\theta) =& \frac{a}{8G}\left(\frac{r}{a}(\kappa+1)\cos(\theta) + 2\frac{a}{r}\left[(1+\kappa)\cos(\theta)+\cos(3\theta)\right] - 2\frac{a^3}{r^3}\cos(3\theta)\right), \\
u_y(r,\theta) =& \frac{a}{8G}\left(\frac{r}{a}(\kappa-3)\sin(\theta) + 2\frac{a}{r}\left[(1-\kappa)\sin(\theta)+\sin(3\theta)\right] - 2\frac{a^3}{r^3}\sin(3\theta)\right),
\end{aligned}
\tag{28}
$$

where G is the shear modulus and κ indicates the Kolosov constant. For plane stress conditions $\kappa = (3-\nu)/(1+\nu)$.

The numerical analyses have been performed by investigating three different discretization levels with 65, 341 and 2133 nodes. Fig. 10 shows the discretization with 65 nodes. The figure indicates, that the node density increases with decreasing distance to the hole. This is similar for all three discretizations. The following discretization schemes are used for the investigations:

- Three-node (CST), four-node (Q4) and nine-node (Q9) iso-parametric finite elements with linear, bilinear and quadratic shape functions

- MLS approach with circular nodal influence domains (CD) and a given number of influencing nodes (IN) for each node

- MLS approach with circular nodal influence domains using the scaled maximum distance to the natural neighbor nodes (NN)

- MLS approach with adapted nodal influence domains (AD) using scaled interpolated nodal distances

The number of influencing nodes is chosen as: 9 nodes for the linear basis, 12 nodes for the bilinear basis and 30 nodes for the quadratic basis. The scaling factor β is taken as $\beta = 1.3$ for the linear basis, $\beta = 1.5$ for the bilinear basis and $\beta = 2.5$ for the quadratic basis.

In Fig. 11 the number of influencing nodes and the interpolated nodal influence radius at the interpolation points is shown for the MLS approach with linear basis and the discretization using 65 nodes. The figure clearly indicates, that the number of influencing nodes is nearly
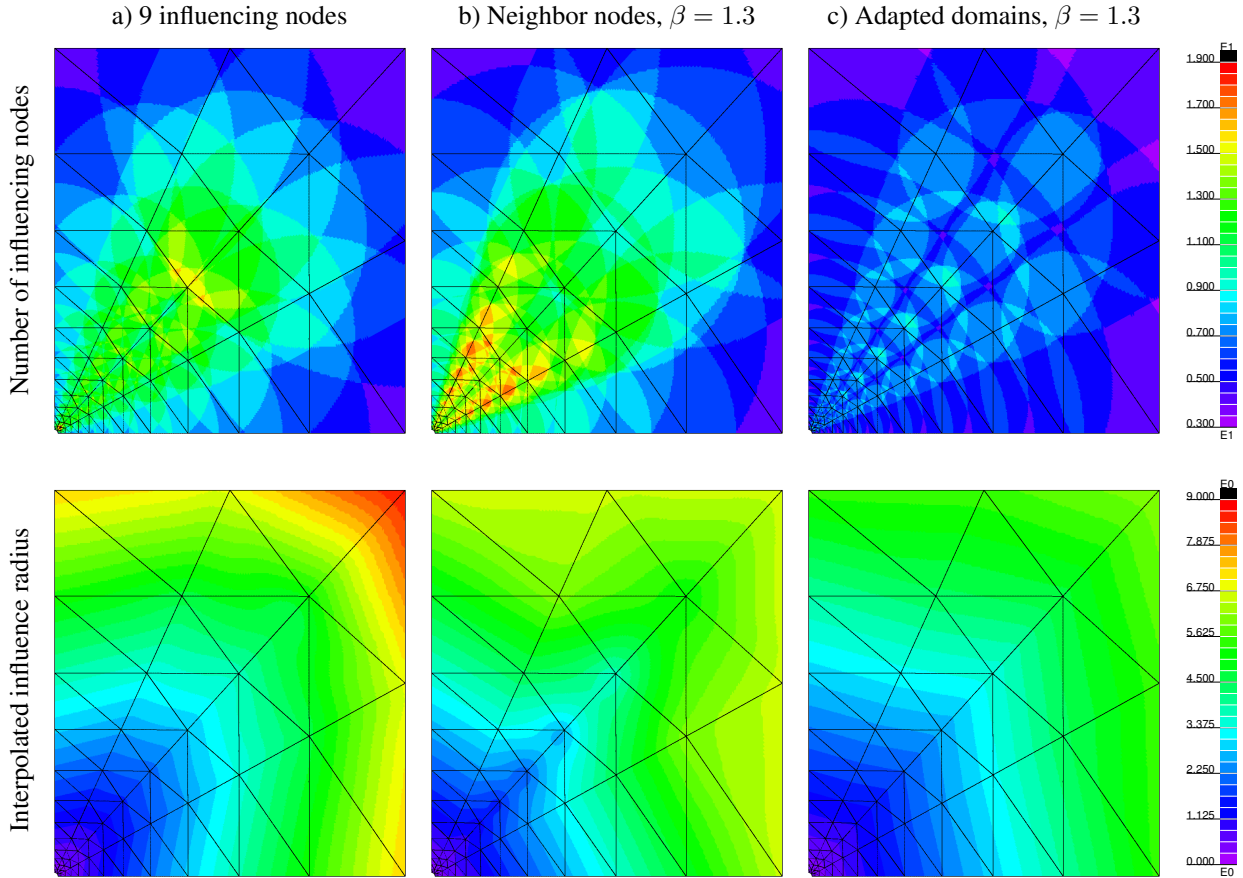

Figure 11: Number of influencing nodes and interpolated nodal influence radius by using a) a fixed number of nodes in the influence domain of each node, b) using the maximum distance to the natural neighbor nodes and c) using adapted nodal influence domains with interpolated radii

similar for case a) and case b), whereby for the first case a concentration close to the hole can be seen, which is caused by the large influence radii of the corner nodes. By using the adapted nodal influence domains, the number of influencing nodes is much smaller in the middle part and almost uniform in the whole structure.

In Table 3 the influence of the different approaches on the computational effort is given for the coarsest discretization. All meshless calculations have been carried out using the regularized spline weighting function and 25 Gauss integration points per triangular integration cell. The table shows, that the application of the adapted nodal influence domains, which leads to a reduced number of influencing nodes for the most integration points, enables an remarkable efficiency increase for the shape function and stiffness matrix computation and even for the solution of the global system of equations. The additional numerical effort for the interpolation of the nodal influence radius leads at the end to a large reduction of the total numerical costs. This is much more significant for a nonlinear analyses, where the shape functions have to be com-

13

			Number of operations [10^6]				
			a) Weights	b) Shapes	c) Stiffness	d) Solution	Total
MLS-IN-CD	Linear	9 nodes	40.41	12.17	43.07	0.99	96.64
MLS-IN-CD	Bilinear	12 nodes	61.64	19.24	78.37	1.12	160.37
MLS-IN-CD	Quadratic	30 nodes	324.51	82.23	569.55	1.26	977.55
MLS-NN-CD	Linear	$\beta = 1.3$	36.65	13.31	59.23	0.96	110.15
MLS-NN-CD	Bilinear	$\beta = 1.5$	58.07	21.77	122.16	1.13	203.13
MLS-NN-CD	Quadratic	$\beta = 2.5$	398.45	92.79	827.33	1.26	1319.83
MLS-NN-AD	Linear	$\beta = 1.3$	43.88	9.13	15.86	0.63	69.50
MLS-NN-AD	Bilinear	$\beta = 1.5$	55.16	13.45	24.67	0.87	94.15
MLS-NN-AD	Quadratic	$\beta = 2.5$	143.97	63.62	181.78	1.15	390.52

Table 3: Required computational effort for a) the neighbor search and the weighting function calculation, b) the shape function computation, c) the stiffness matrix calculation and d) the solution of the global system of equations

puted only after each discretization update and the stiffness matrix calculation and the solution of the global system have to be performed in every iteration step.

Finally the convergence and the accuracy of the different approaches are analyzed using the averaged relative error of the u_y displacement at point A and the u_x displacement at point B

$$\eta = \frac{1}{2} \left| \frac{\tilde{u}_y^A - u_{y,exact}^A}{u_{y,exact}^A} \right| + \frac{1}{2} \left| \frac{\tilde{u}_x^B - u_{x,exact}^B}{u_{x,exact}^B} \right| . \tag{29}$$

In Fig. 12 the error value η is shown for the FEM and MLS calculations depending on the discretization level. The figure indicates, that in general all approaches lead to similar results. Generally the MLS errors using the adapted nodal influence domains are slightly higher than these using the circular domains, nevertheless the results are still better as these obtained with the comparable finite elements.

6 CONCLUSIONS

In this paper two enhancements of the classical Moving Least Squares approach have been presented. The first one is a non-singular interpolating weighting function, which leads to MLS shape functions fulfilling the interpolation condition exactly. This enables a direct application of essential boundary conditions without additional numerical effort. Furthermore this weighting function leads to results, which are much more independent of a distortion of the nodal configuration and the size of the influence domain as these obtained with classical weighting types. Nevertheless, for practical applications the results are similar as these obtained with the regularized weighting type presented by the authors in previous publications.

The second approach, which was presented in this paper, is the adaptation of the nodal influence domains according to the nodal configurations. For this purpose the influence radius is interpolated depending on the direction from the distances to the natural neighbor nodes. This leads to a more uniform and reduced number of influencing nodes for systems with varying node density than the classical circular influence domains. It could be shown, that the small additional numerical effort for interpolating the influence radius leads to remarkable reduction of the total numerical cost in a linear analysis while obtaining similar results. For nonlinear calculations this advantage would be even more significant.

ACKNOWLEDGEMENT

REFERENCES

[1] T. Belytschko, Y. Y. Lu, and L. Gu. Element-free Galerkin methods. *International Journal for Numerical Methods in Engineering*, 37:229–256, 1994.

[2] P. Lancaster and K. Salkauskas. Surface generated by moving least squares methods. *Mathematics of Computation*, 37:141–158, 1981.

[3] I. Kaljevic and S. Saigal. An improved element free Galerkin formulation. *International Journal for Numerical Methods in Engineering*, 40:2953–2974, 1997.

[4] M. Kunle. *Entwicklung und Untersuchung von Moving Least Square Verfahren zur numerischen Simulation hydrodynamischer Gleichungen*. PhD thesis, Eberhard-Karls-University Tübingen, Germany, 2001.

[5] U. Häussler-Combe. *Elementfreie Galerkin-Verfahren: Grundlagen und Einsatzmöglichkeiten zur Berechnung von Stahlbetontragwerken*. Habilitationthesis, University of Karlsruhe, Germany, 2001.

[6] T. Most and C. Bucher. A Moving Least Squares weighting function for the Element-free Galerkin Method which almost fulfills essential boundary conditions. *Structural Engineering and Mechanics*, 21(3):315–332, 2005.

[7] J. Dolbow and T. Belytschko. Numerical integration of the galerkin weak form in meshfree methods. *Computational Mechanics*, 23:219–230, 1999.

[8] M. K. Alves and R. Rossi. A modified element-free Galerkin method with essential boundary conditions enforced by an extended partition of unity finite element weight function. *International Journal for Numerical Methods In Engineering*, 57:1523–1552, 2003.

[9] S. H. Lo. Delaunay triangulation of non-convex planar domains. *International Journal for Numerical Methods in Engineering*, 28:2695–2707, 1989.

[10] P. J. Green and R. R. Sibson. Computing dirichlet tessellations in the plane. *The Computer Journal*, 21:168–173, 1978.

[11] D. Roos. *Approximation und Interpolation von Grenzzustandsfunktionen zur Sicherheitsbewertung nichtlinearer Finite-Elemente-Strukturen*. PhD thesis, Bauhaus-University Weimar, Germany, 2002.

[12] D. Shepard. A two-dimensional interpolation function for irregular spaced data. In *Proc. 23rd Nat. Conf. ACM*, pages 517–24. 1968.

[13] R. Sibson. A vector identity for the dirichlet tesselation. In *Mathematical Proceedings of the Cambridge Philosophical Society 87*, pages 151–155, 1980.

[14] J. F. Unger. Development of an efficient algorithm for the application of the Natural Neighbor Interpolation for crack growth simulations. Diploma thesis, Bauhaus-University Weimar, Germany, 2003.

[15] S. P. Timoshenko and J. N. Goodier. *Theory of Elasticity (Third ed.)*. McGraw Hill, New York, 1970.
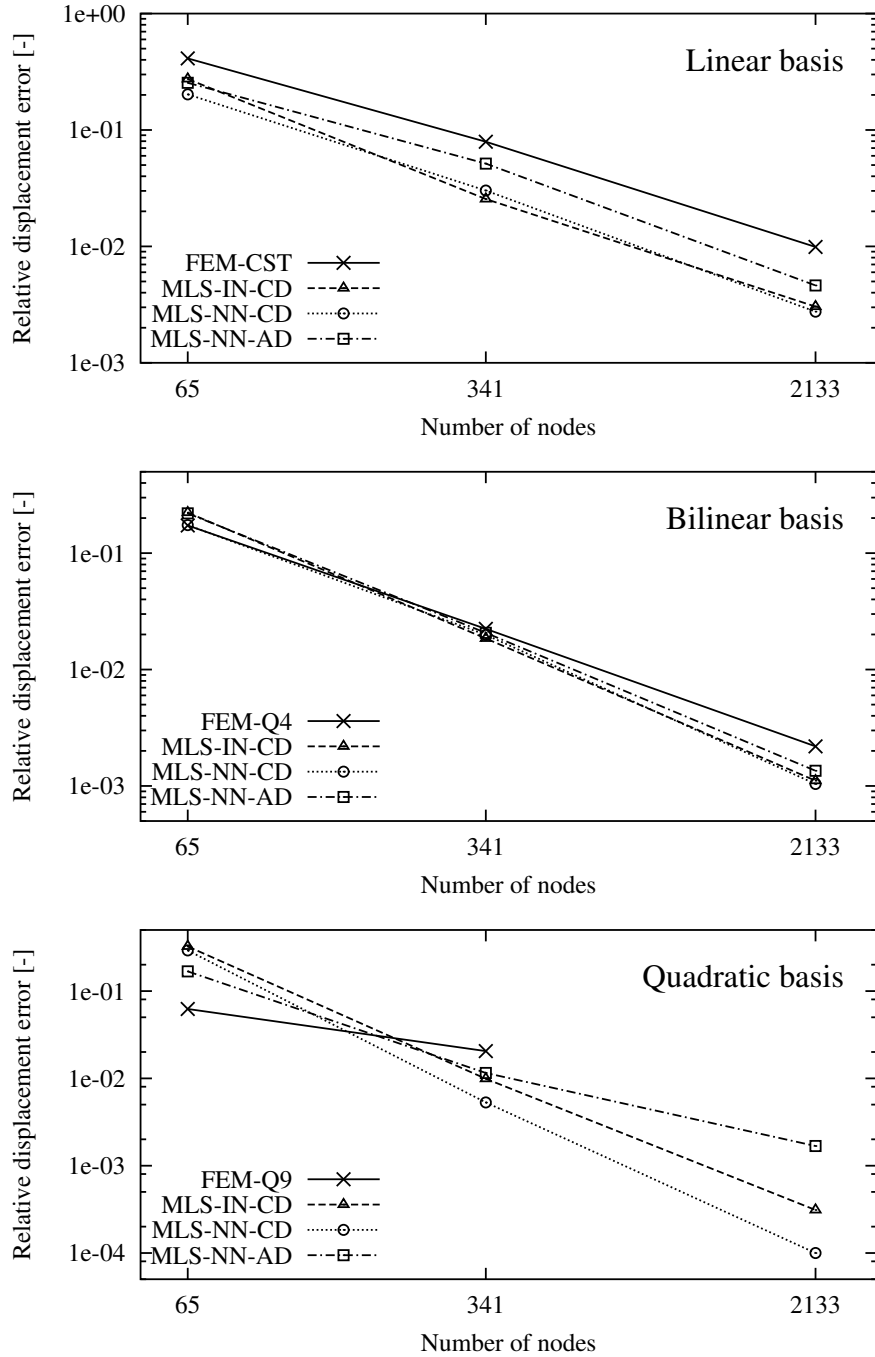
Figure 12: Relative displacement error η depending on the discretization level for the infinite plate with a hole